

SEGMENTED INTERPOLATION ALONG THE COASTLINE FOR AVHRR NOAA IMAGES

Maurizio Tommasini, Gabriele Poli and Pier Franco Pellegrini

DET – Telecommunications and Electronics Department, University of Florence, Florence, Italy
{m.tommasini / pf.pellegrini / g.poli}@labtele.det.unifi.it

ABSTRACT

This paper presents an innovative interpolation method applied to remotely sensed data, based on an appropriate check of the pixels that need interpolation and of the data points used for interpolation. The aim of the method is to project remotely sensed data on a Mercator grid (Datum WGS84) to obtain a highly defined raster image especially along the coastline, where the sensor footprint includes a portion of sea and a portion of land simultaneously.

This interpolation method is mainly based on checking the points acquired by satellite sensor before computing interpolation. This check is based on a criterion of suitability for interpolation depending upon satellite points and regular Mercator grid pixels. For this purpose, we defined some fixed geographical area formats that were accurately segmented into land-pixels and sea-pixels. This result was possible by developing a sub-pixel precise data navigation method for AVHRR (Advanced Very High Resolution Radiometer) NOAA remote sensed data which uses automatic geographical correction. Moreover, considering the dimensions and the shape of AVHRR sensor lobe, for each satellite point the closeness to the coast is taken into account in order to identify mixed points.

Considering land-sea classification, closeness to the coast of satellite points and land-sea classification of Mercator raster image pixels, suitable points for interpolation are selected while unsuitable points are calculated again using close suitable points. The results show a remarkable enhancement in image definition along the coastline.

This method was optimised on a regional scale, in the areas of the Tuscan Sea and Tuscan Archipelago, and its operation was verified using SST (Sea Surface Temperature) images obtained with AVHRR data and also with artificial data. Such testing was carried out through a numerical comparison between images obtained using segmented and ordinary interpolation and also *in situ* data where present.

Keywords: Interpolation, segmentation, coastline, AVHRR, SST.

INTRODUCTION

The aim of this work is to design an algorithm that allows sea observation from satellite passive remote sensors, especially near the coastline. The image of interest is obtained by bilinear interpolation over a regular Mercator WGS84 grid; as shown in Figures 1 and 2, every grid pixel Q (indicated with grid coordinates u,v [pixel]) is interpolated using four points P acquired by satellite (those points are indexed with j,i and their geographical coordinates, longitude and latitude, are indicated with x,y). For this purpose, a new bilinear interpolation algorithm has been developed to resample sea grid pixels near to the coast, because of the particular interest in coastal zones, and thanks to precise image navigation.

The aim of the present algorithm, that can be called *segmented interpolation algorithm*, is to remove, or at least significantly reduce the effect of the land along coastlines, which appear when an ordinary bilinear interpolation procedure is used. This goal is quite important to attain because the more this land effect is reduced, the more the interpolation grid pixel resolution is honoured by the interpolation procedure. This effect is due to the fact that near to the coast a pixel u,v of interest, geolocated on the sea, can be interpolated using one or more points x,y , explored by a passive

satellite sensor (Figure 2), geolocated on the land or contaminated by the proximity to the land (mixed sea points, (1,2). In the image obtained with ordinary interpolation, such as from the data of AVHRR channel 3 (Figure 9), the coastlines are not clearly defined and there is not a sharp division between the land and the sea (as shown also by (1,3,4,5).

The main difference between the ordinary and the segmented algorithm is an appropriate check of the geolocation of the pixel u,v to be interpolated, and of the points x,y of the quadrilateral that surround the pixel (Figure 1). The algorithm also checks if the points of the reference quadrilateral are contaminated by the proximity to the land; this check is achieved through an approximate model of the satellite footprint (see below). When interpolating a sea pixel, if some of the points of the quadrilateral are geolocated on land or contaminated, the algorithm corrects the z coordinate of these quadrilateral points using the nearby unmixed points' z coordinate. Then the pixels u,v are interpolated as in the ordinary algorithm. Practically, the aim of the method is to resample sea grid pixels using only unmixed sea image points.

DESCRIPTION OF THE ALGORITHM

The representation of the physical parameter retrieved over the sea (e.g., SST) is considered to be slowly variable with respect to satellite points. In other words, it can be said that the spatial density of satellite points satisfies the sampling theorem hypothesis. Such conditions, verified in practice for the Tuscan Sea region, allow the interpolation of the physical parameter's value everywhere in the investigated surface; of course, interpolation can be done according to a predetermined pixel grid. For this work a Mercator grid was chosen for the purpose. In particular, two different grid steps were defined: about 140 metres (for Tuscan Archipelago geographical format, see Table 3 and Figure 7) and about 280 metres (for Tuscany geographical format, see Table 3 and Figure 17).

In the interpolated image to be obtained, the pixels' spatial accuracy is highly dependent on satellite points geolocation. For the geolocation, coincidence between the remotely sensed image and GCPs (Ground Control Points) was not checked considering single satellite points. After registering satellite data on the Mercator grid, geolocation was achieved through bidimensional cross-correlation, within appropriate templates including a relevant portion of coastline, between the satellite image and the true vectorial coastline data registered on the same grid.

It was proved that, with cross-correlation methods, referring to the Mercator interpolation grid, geolocation can be realized with an accuracy of at least a quarter of the sensor lobe dimension (i.e., about 275 metres for AVHRR NOAA). Therefore, using a grid step of 140 metres (e.g., for Tuscan Archipelago format) to interpolate AVHRR data does not mean that the resulting image will have a spatial resolution of 140 metres.

The interpolation of a generic pixel $Q(u,v)$ of the Mercator grid is made according to the points $P(x,y)$ acquired by the satellite sensor that surround it (Figure 1). Satellite points form a box that can be called reference quadrilateral for the interpolation of the pixel $Q(u,v)$. According to the obtained satellite data geolocation and considering the coastlines, it is possible to work out a *land-sea* classification for the grid pixels to be interpolated and for the points acquired by satellite; moreover it is possible to define a contamination index (cn) for satellite points which takes into account their proximity to the coastline (Figure 3).

The developed segmented algorithm performs the following actions:

1. land-sea classification for the interpolation grid pixel $Q(u,v)$ and for the satellite points $P(x,y)$ of the reference quadrilateral for the interpolation (Figure 1);
2. calculation of the contamination index (cn , see Eq. (1)) for the satellite points $P(x,y)$ of the reference quadrilateral for the interpolation (Figure 3);
3. suitability criterion: z coordinate of points $P(x,y)$, that are unsuitable for the resampling of the grid pixel $Q(u,v)$, is reprocessed using the closest suitable points' z coordinates (Figure 4);
4. bilinear interpolation of the grid pixel $Q(u,v)$.

To perform a land-sea classification for grid pixels, a numerical flag ($Class_{TM}$), which indicates the geolocation of pixel, is assigned to each of them, according to the coastline of the selected geographical sub-area (e.g., Tuscany format or Tuscan Archipelago format, see Table 3). Land-sea classification for satellite points is carried out considering the grid pixel that is determined by the sensor lobe centre position. If this grid pixel is a land, coast or sea pixel, the same is assumed for the satellite point (Figure 2). In other words, *land-sea* classification for a satellite point x,y is held identical, with acceptable approximation, to the closest grid pixel u,v classification (Table 2).

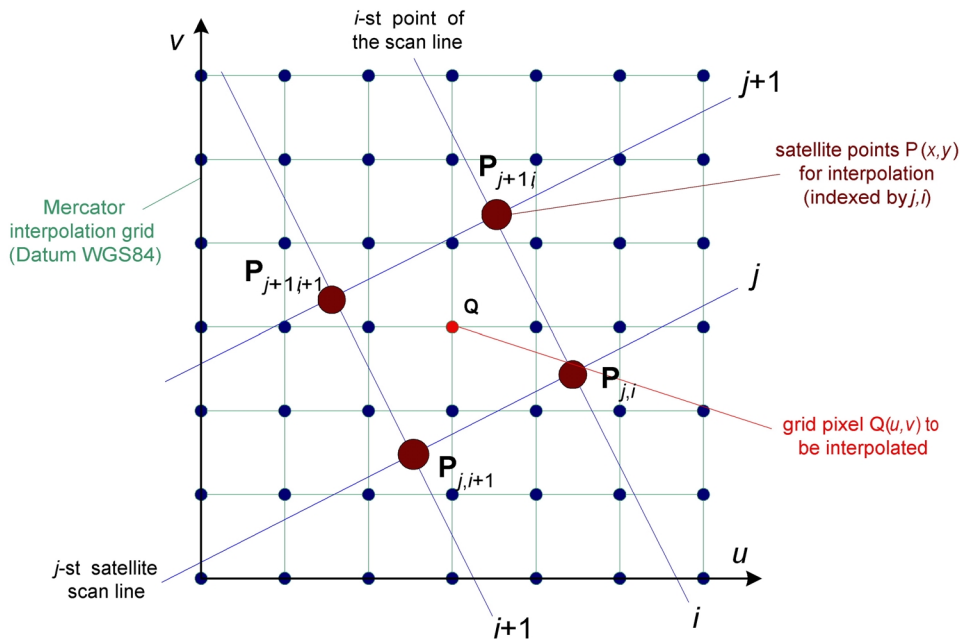


Figure 1: Satellite points $P(x,y)$ (indexed by j,i , where x,y are longitude and latitude respectively) of the reference quadrilateral for the interpolation of a generic pixel $Q(u,v)$ located on a regular grid, normally in Mercator projection.

Table 1: Land-sea classification of grid pixels: assignment of land-sea flag $Class_{TM}$ to pixels u,v of the resampling grid according to the coastline of the selected geographical format (Figure 2).

$Class_{TM}$	land-sea classification for pixels $Q(u,v)$
0	Coast
1	Land
2	Sea

Table 2: Land-sea classification of satellite points: assignment of land-sea flag $CITM$ to points x,y acquired by satellite (Figure 2). E.g., $CITM = -1$ if point x,y falls outside the limits of the selected geographic format.

$CITM$	land-sea classification for points $P(x,y)$
0	Coast
1	Land
2	Sea
-1	not classifiable on the basis of the closest grid pixel u,v

To calculate the contamination index (cn , see Eq. (1)) for a satellite point (e.g., point P_0 in Figure 2), sensor lobe features have to be taken into account. In this work, we focused on the sensor AVHRR on board the NOAA satellites. AVHRR's sensor lobe is characterized by a pseudo-elliptical shape, whose major axis measures about 1.1 km (6). Referring to the Mercator interpolation grid, it is possible to approximate this shape using a square matrix with an odd number of pixel sides (so

that the matrix refers to the central pixel, see Figure 3) centred on the pixel that is closest to the point whose cn has to be computed (Figure 3). Approximation square matrix side (LM) varies according to the selected geographical format, depending on the effective size (in km) of the image pixel.

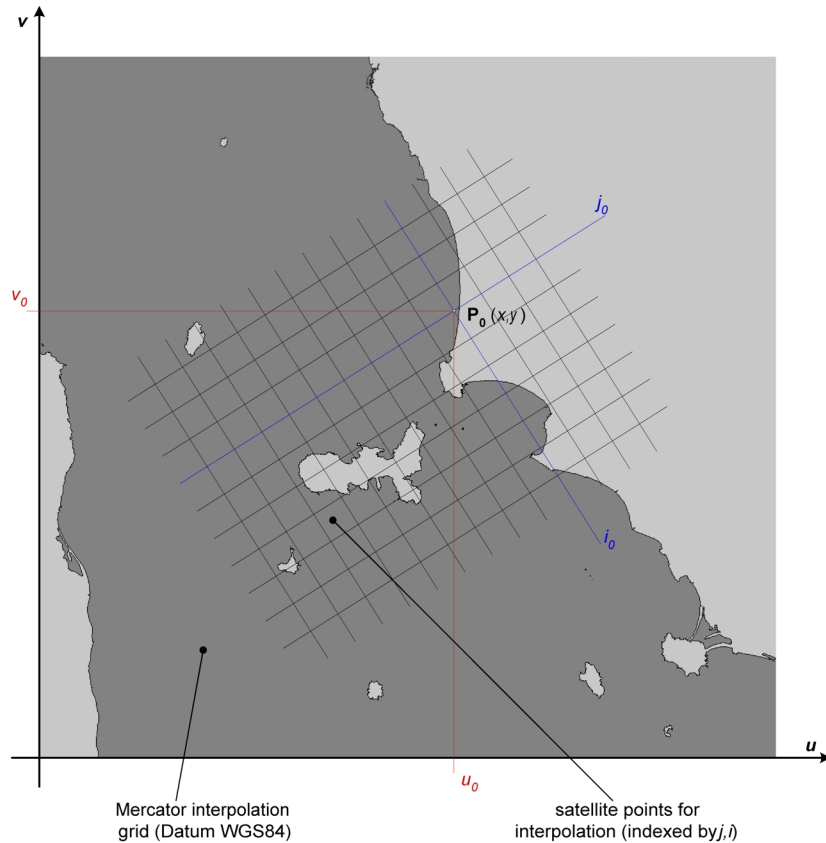


Figure 2: Reference system for Mercator coordinates and Land-sea classification for satellite points: land-sea classification for the point $P_0(x, y)$ is held identical, with acceptable approximation, to the classification of the closest grid pixel u_0, v_0 .

Referring to the central pixel u_0, v_0 (Figure 3), the contamination index (cn) for the sea satellite point P_0 is computed using the value of $ClassTM$, LM , N , associated to that pixel (see Table 1 and Figure 3), and the land-sea classification of the point P_0 ($CITM$, see Table 2); for a generic satellite point P_0 the adopted formula for cn is:

$$cn = \begin{cases} \frac{N_{tot} - N}{N_{tot}}, & \text{if } CITM = 0 \text{ or } CITM = 1 \\ \frac{N}{N_{tot}}, & \text{if } CITM = 2 \\ -1, & \text{if } CITM = -1 \end{cases} \quad (1)$$

- where:
- cn contamination index for the satellite point P_0 of interest;
 - $CITM$ land-sea classification flag for the satellite point P_0 of interest;
 - $N_{tot} = LM^2 - 1$ total number of checked pixels in the approximation matrix referred to the grid pixel u_0, v_0 (Figure 3);
 - $N = N_t + N_c$ land or coast pixel number N included in the approximation matrix referred to the grid pixel u_0, v_0 (it is given by the sum of land pixels number and coastline pixels number, see Figure 3).

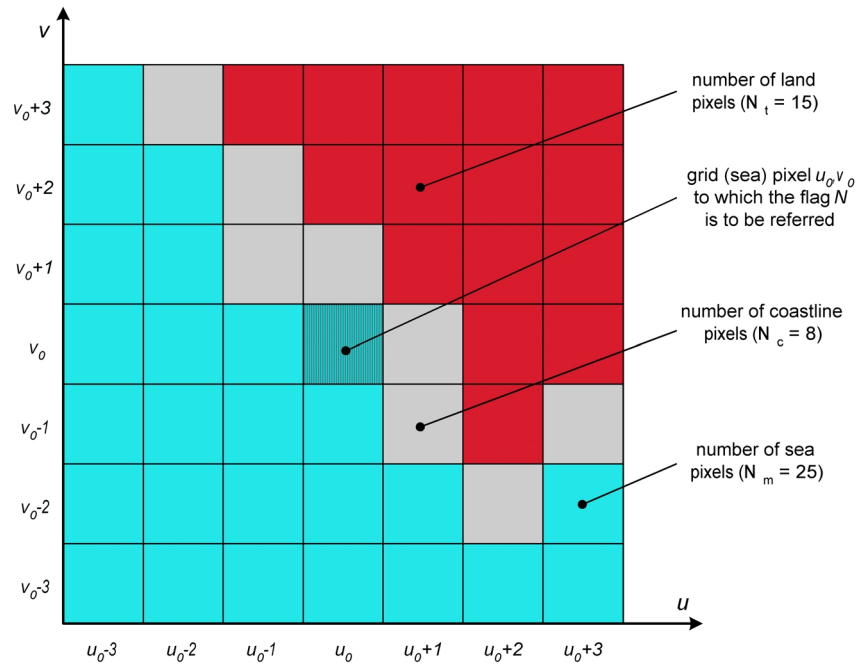


Figure 3: Example of contamination index (cn) computation for a sea satellite point P_0 : land-coast pixel number (N), included in the sensor lobe approximation matrix, is considered; the matrix refers to the grid pixel u_0, v_0 , which is the closest pixel to point P_0 . In this example $LM = 7$ (this matrix size is adopted for the Tuscan Archipelago format in order to approximate AVHRR sensor lobe dimensions), hence the number of checked pixels in the matrix is $N_{tot} = 48$; then, having $N = 23$, $cn = 0.4791$.

Given a grid pixel to be interpolated, its *land-sea* classification flag (*ClassTM*, see Table 1) and setting some threshold value (cn_s) for the contamination index, beyond which a point is regarded as a mixed point, satellite points (characterized by *CITM* and cn , see Table 2 and Figure 3) are divided into suitable (for pixel interpolation) and unsuitable according to this criterion:

An image point x, y of the reference quadrilateral is suitable to interpolate a grid pixel u, v if it has the same land-sea classification of the grid pixel and if the value of its contamination index is below the fixed threshold (cn_s); the criterion is equivalent to the conditions:

$$CITM = ClassTM \tag{2}$$

$$cn < cn_s \tag{3}$$

where:

- CITM* land-sea classification flag for point x, y ;
- ClassTM* land-sea classification flag for grid pixel u, v to be interpolated;
- cn contamination index for the satellite point x, y ;
- cn_s threshold value (cn_s) fixed for the contamination index.

Suitable points, according to Eqs. (2) and (3), are used for the interpolation; on the other hand, unsuitable points maintain their x, y coordinates but their z coordinate is reprocessed using the closest suitable points' z coordinates. The points taken into consideration for reprocessing are those placed along one of the eight possible directions, determined also by an index (in red between brackets in Figure 4), ranging from 0 to 7 (there are three points in each direction, see Figure 4). The reprocessing direction is chosen between the eight directions (Figure 4) following these criteria (in order of importance):

1. number of suitable points along the direction;
2. average distance of suitable points from unsuitable point whose z is to be reprocessed;
3. type of direction (direction nr.1 is preferred, then nr. 2, 3, and so on; see Figure 4).

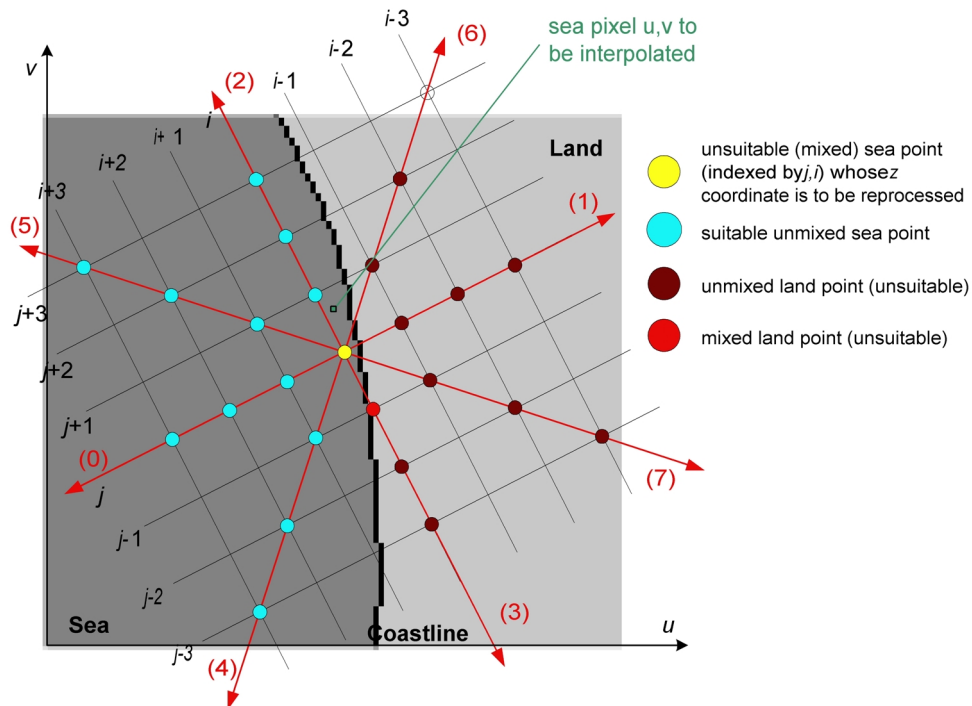


Figure 4: Reprocessing of the z coordinate of a satellite point unsuitable for the resampling of a sea pixel u, v . The value of z coordinate is reprocessed using the closest suitable points' z coordinates; the closest points are those placed along the selected direction.

The z coordinate value of a satellite point unsuitable for the interpolation is reprocessed using the closest suitable points' z coordinates; the closest points are those placed along the selected direction. If, unfortunately, there are not any suitable points along the eight directions, the unsuitable point maintains its z coordinate. After such a reprocessing, the interpolation of the grid pixels is achieved following the same method as the ordinary algorithm. Before interpolating one more grid pixel, the z coordinates of the unsuitable points take on their original value, so that the algorithm performs a new z coordinate point reprocessing according to the new grid pixel to be interpolated.

In describing the algorithm, examples are given considering sea grid pixel to be interpolated. However, the algorithm performs the same if land grid pixels have to be interpolated; moreover, the contamination index for a land satellite point, which is near to the coastline, is computed (see Eq. (1)) taking into account the number of sea pixels (instead of land or coastline pixels, as in Figure 3) within the approximation matrix.

RESULTS

The proposed algorithm operation was verified using artificial data as well as AVHRR NOAA sensor data; *in situ* data were also used. Testings were based on visual and quantitative comparisons between interpolated images (obtained with ordinary and segmented method), synthetic images and *in situ* data where present.

Table 3: Geographical limits of the selected geographical formats (Tuscan Archipelago and Tuscany). Mercator grid step for image interpolation is about 140 m for Tuscan Archipelago and 280 m for Tuscany (Kmpp constant in the table).

Geographical format	longitude and latitude of SW image corner (Lon _{SW} , Lat _{SW}) /deg	longitude and latitude of NE image corner (Lon _{NE} , Lat _{NE}) /deg	Pixel physical dimension (Kmpp) / km/pixel
Tuscan Archipelago	09°24' E, 42°12' N	11°24' E, 43°36' N	0.141111109
Tuscany	09°12' E, 42°12' N	12°24' E, 44°30' N	0.282222218

The selected geographical sub-areas were the Tuscan Archipelago and Tuscany; according to these sub-areas two formats for elaboration (Tuscan Archipelago and Tuscany) were defined. In Table 3 there are the geographical limits of the considered sub-areas and the pixel dimension of the obtained images (*Kmpp* constant).

Two different interpolation grid resolutions (*Kmpp*) were chosen in order to test more completely algorithm results.

Results with artificial data

Algorithm testing with artificial data was carried out creating a synthetic raster SST image, according to the Tuscan Archipelago geographical format (see Table 3 and Figure 7). This synthetic image presents a linear temperature gradient along the direction locally orthogonal to the coastline (Figure 6). Taking into account AVHRR’s sensor scansion lobe and the geo-location data of a NOAA satellite real pass, SST geo-located data, whose interpolation would generate the synthetic raster image, are retrieved. Retrieved SST data are then interpolated using both an ordinary and a segmented algorithm. Figure 5 illustrates how the testing was carried out.

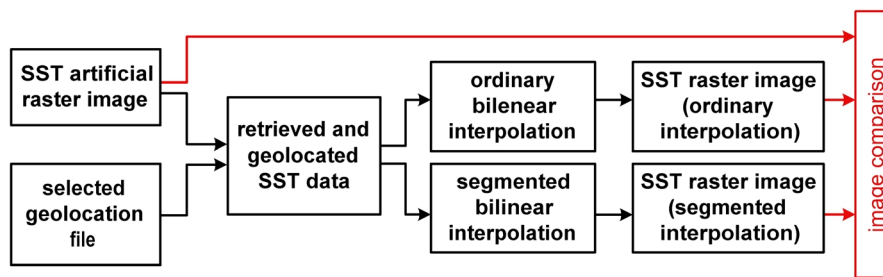


Figure 5: Flow diagram for testing the results obtained with a segmented interpolation algorithm on artificial SST data.

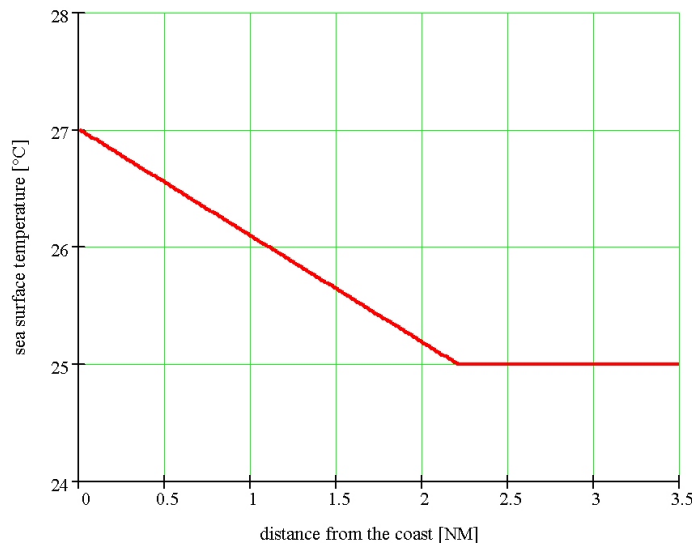


Figure 6: SST synthetic image linear gradient along the direction locally orthogonal to the coastline. Reference SST values are typical during summertime in the Tuscan Archipelago; distance from the coast is in nautical miles.

For the comparison of the obtained raster images, some sub-windows of the *Tuscan Archipelago* format were selected including the coastline (Figure 7). For each of the sub-windows the mean absolute error (MAE) of the interpolated images referring to the synthetic image was calculated. MAE calculation is done according to Eq. (4) and takes into account only the grid pixels modified by the segmented interpolation algorithm in comparison with the ordinary algorithm.

$$MAE = \sum_{u,v} \frac{|\hat{z}_{u,v} - z_{u,v}|}{M} \tag{4}$$

where: MAE mean absolute error
 u,v grid coordinates of sea pixels (in the sub-window) modified by segmented interpolation algorithm in comparison with ordinary algorithm
 $z_{u,v}$ pixel value of coordinates u,v in the synthetic image
 $\hat{z}_{u,v}$ pixel value of coordinates u,v in the interpolated image
 M number of sea grid pixels taken into account in the sub-windows (only those modified by the segmented interpolation algorithm in comparison with the ordinary algorithm)

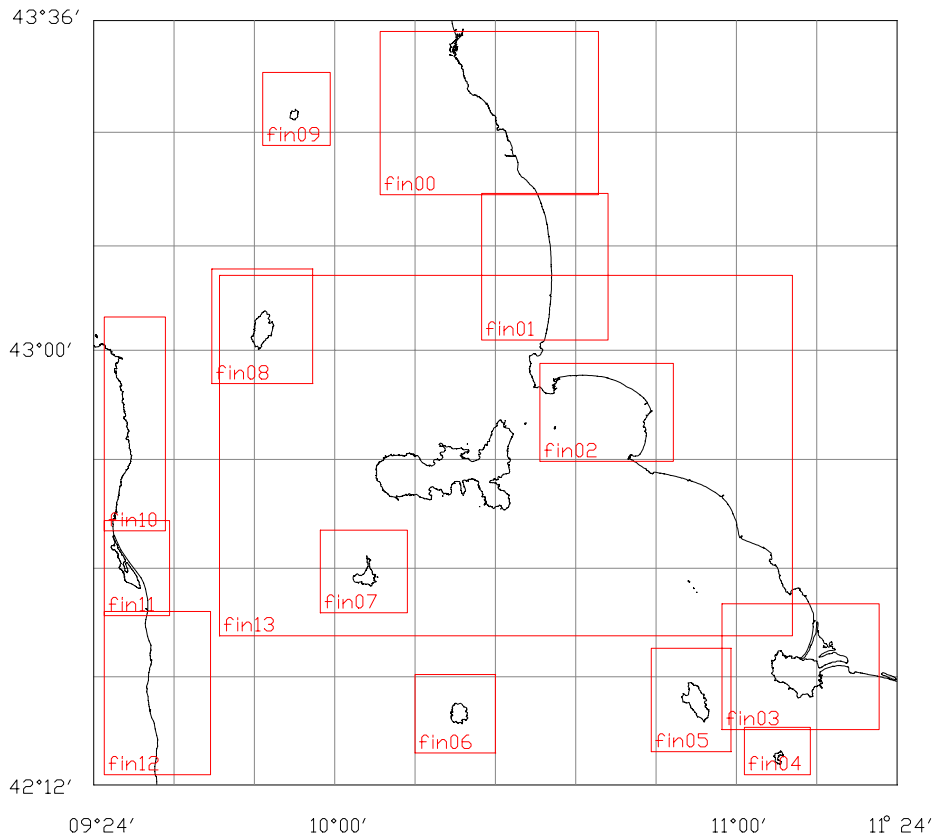


Figure 7: Sub-windows of the Tuscan Archipelago geographical format, selected for the comparison, through MAE calculation, between images obtained with ordinary and segmented algorithms.

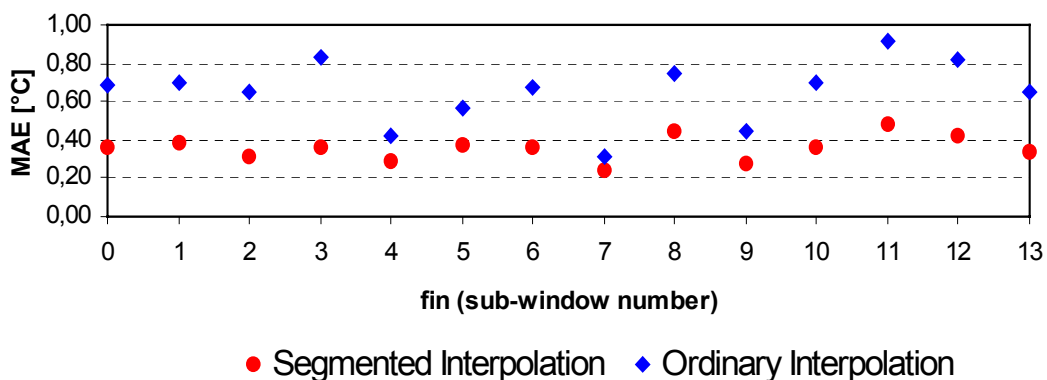


Figure 8: Mean Absolute Error (MAE) between interpolated artificial data and the original synthetic raster image in the selected sub-windows (Table 4): comparison between segmented and ordinary interpolation; on x-axis there is the sub-window number (fin) (see Figure 7).

Table 4: Comparison between interpolated images and synthetic image. fin: sub-window number; (u_{SW}, v_{SW}): sub-window SW corner; (u_{NE}, v_{NE}): sub-window NE corner; M: number of pixels considered in sub-window; M_{tot} : number of pixels in sub-window; %: percentage of M over M_{tot} ; MAE_s , MAE_o : MAE in images obtained with segmented and ordinary interpolation (see Figure 7).

fin	u_{SW}	v_{SW}	u_{NE}	v_{NE}	M	M_{tot}	%	MAE_s	MAE_o	$MAE_o - MAE_s$
fin00	0412	0850	0726	1085	002411	074340	003.243	0.364562	0.682024	+ 0.317462
fin01	0558	0641	0740	0852	001580	038796	004.073	0.388911	0.693051	+ 0.304139
fin02	0642	0466	0834	0607	002445	027406	008.921	0.315395	0.652564	+ 0.337170
fin03	0904	0080	1130	0261	003726	041314	009.019	0.360282	0.830580	+ 0.470298
fin04	0936	0015	1031	0083	000272	006624	004.106	0.286544	0.422794	+ 0.136250
fin05	0802	0048	0917	0197	001173	017400	006.741	0.374697	0.562276	+ 0.187579
fin06	0462	0046	0578	0159	000428	013338	003.209	0.357897	0.680140	+ 0.322243
fin07	0326	0248	0451	0367	000515	015120	003.406	0.238447	0.318447	+ 0.080000
fin08	0170	0578	0315	0743	000393	024236	001.622	0.450000	0.752901	+ 0.302901
fin09	0243	0921	0340	1026	000378	010388	003.639	0.272540	0.446429	+ 0.173889
fin10	0020	0366	0103	0674	002167	025956	008.349	0.360951	0.698491	+ 0.337540
fin11	0015	0244	0109	0381	001716	013110	013.089	0.480752	0.910006	+ 0.429254
fin12	0015	0030	0168	0250	001509	034034	004.434	0.426508	0.817462	+ 0.390954
fin13	0181	0215	1005	0734	013695	429000	003.192	0.336999	0.652391	+ 0.315392

The results in Table 4 and Figure 8 show that the mean absolute error in evaluating SST is significantly reduced when the segmented algorithm is used instead of the ordinary one. In particular, elaboration carried out on artificial data, referred to the Tuscan Archipelago format and characterized by the gradient of Figure 6, shows an accuracy improvement of SST retrievals of about 0.3°C.

Results with channel 3 AVHRR NOAA counts

The resulting improvement in image definition along the coastline is quite evident considering the images obtained from channel 3 counts of AVHRR sensor. The selected geographical format is *Tuscan Archipelago* (see Table 3 and Figures 9-10), the chosen image is from NOAA16 and is dated July 12, 1997, UTC 12:58; this satellite pass is particularly suitable for the purpose because of the lack of clouds and the ease of accurately geo-locating the image. With ordinary interpolation coastlines are not clearly defined and there is not a sharp division between the land and the sea, but smooth edges and blurred details along the coasts (Figure 9), the result obtained with a segmented interpolation procedure shows instead a remarkable enhancement in image definition along the coastlines (Figure 10).

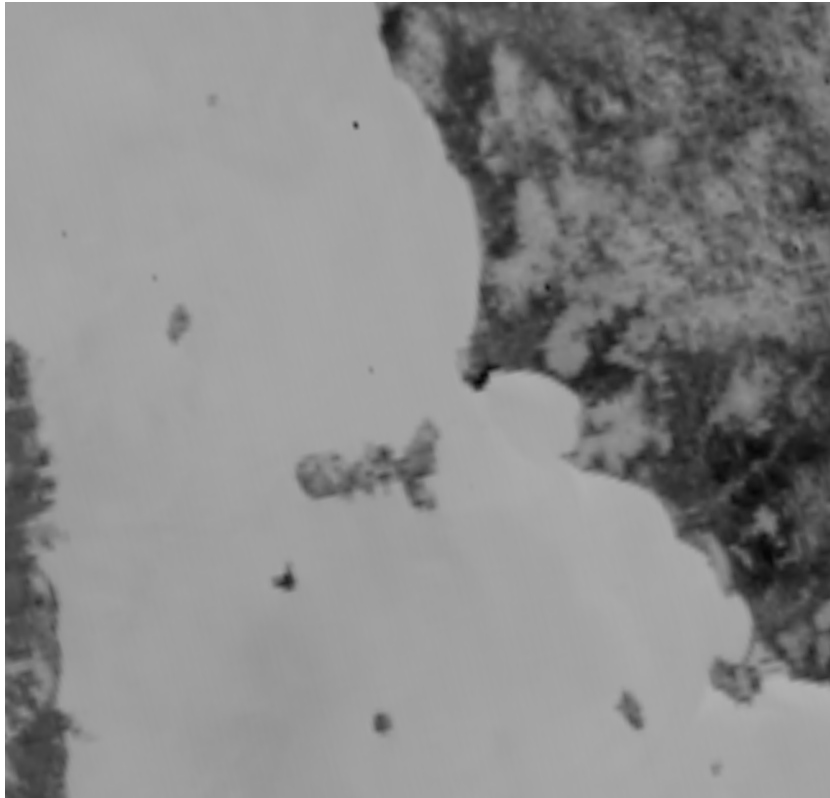


Figure 9: Ordinary interpolation: re-sampled raster image of the Tuscan Archipelago (Table 3), channel 3 AVHRR NOAA16; image of July 12, 1997, UTC 12:58 (see Figure 10 for a comparison with segmented interpolation).

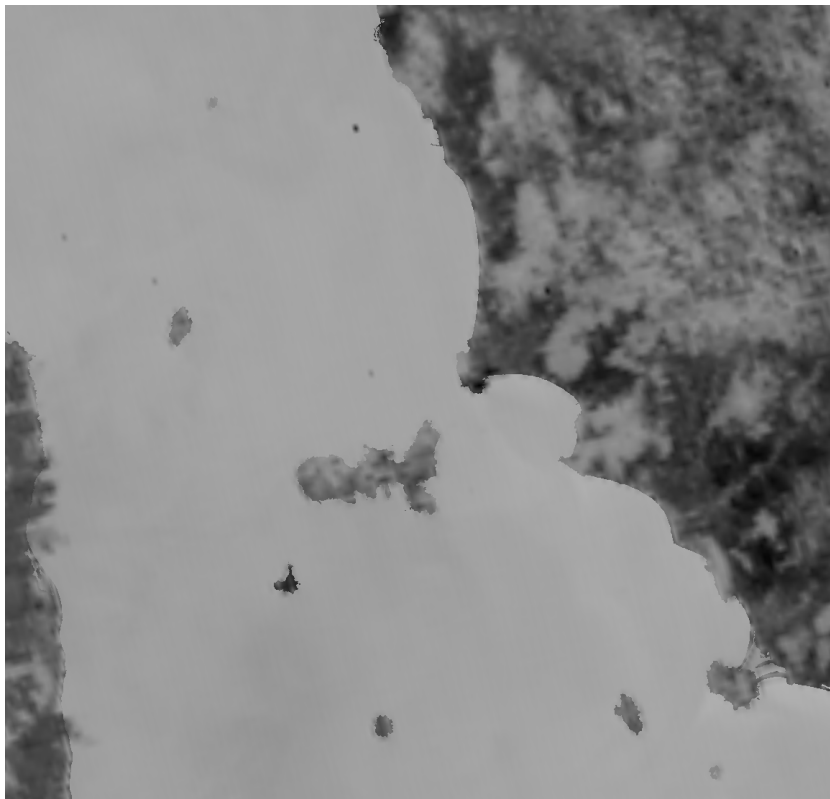


Figure 10: Segmented interpolation: re-sampled raster image of the Tuscan Archipelago (Table 3), channel 3 AVHRR NOAA16; image of July 12, 1997, UTC 12:58 (see Figure 9 for a comparison with ordinary interpolation).

Results with ARPAT *in situ* measurements

A comparison was also made between the *in situ* measurements performed by ARPAT (Environmental Agency of Tuscany) and the SST values, obtained from AVHRR data, with the ordinary algorithm and the segmented algorithm over some sea measurement stations. Figure 11 shows the locations, along the Tuscany coastline, of ARPAT sea measurement stations: the code (two letters) that identifies the station is indicated in brackets. Every measurement station includes three different measurement sites, placed at different distances from the coast. At these sites (as well as some other physical parameters over the sea) the temperature at 0.5 m depth is taken. Measurement sites are characterized by the station code and a number, which indicates site distance from the coast (i.e. the station Carbonifera includes the sites CR05, CR10, CR30 placed respectively at 500, 1000, 3000 m from the coast).

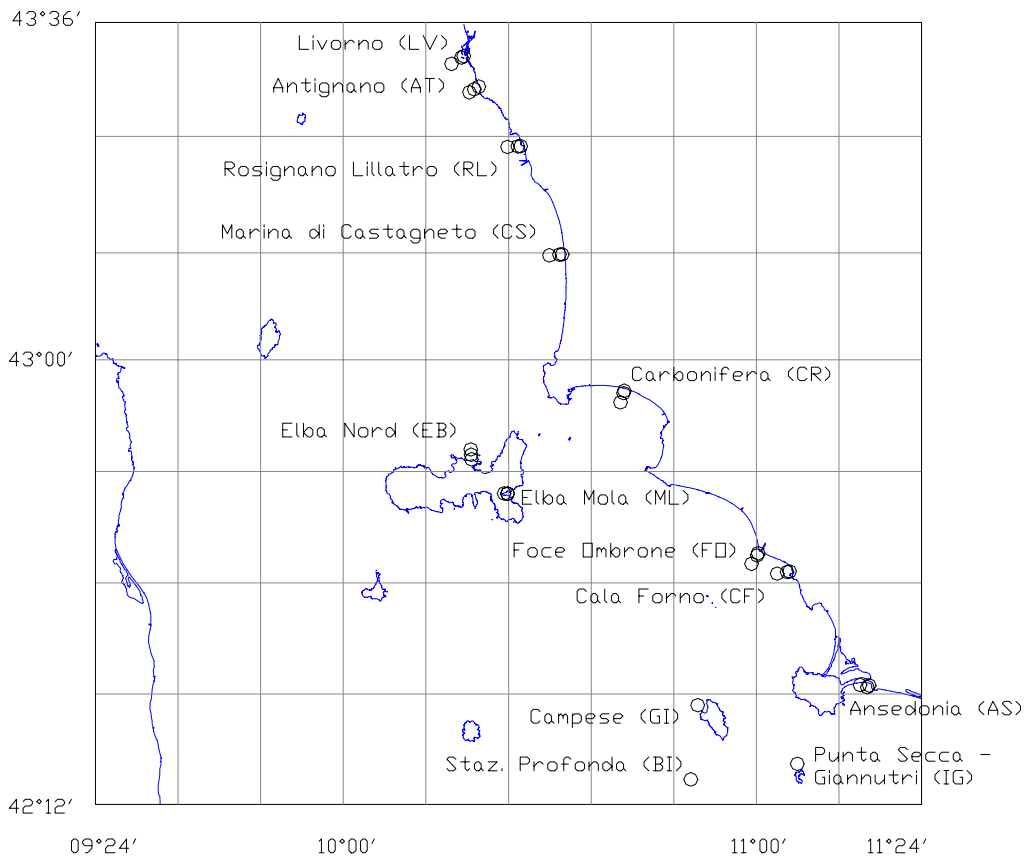


Figure 11: Location and names of ARPAT sea measurement stations. Each of them includes three different measurement sites, placed at different distances from the coast; sea temperature is taken at 0.5 m of depth. Unfortunately for this work it was possible to consider only 3 stations (9 sites, see Table 5): Foce Ombrone, Carbonifera and Elba Nord.

SST images were obtained from AVHRR NOAA14 data of August 1, 2001, using first an ordinary and then a segmented interpolation procedure. Results of such a processing were compared to ARPAT *in situ* measurements. Figure 12 shows the SST image of August 1, 2001, UTC 15:46 obtained with the ordinary interpolation method; Figure 13 shows the same SST image obtained with the segmented interpolation method. Figures 14-15 display an enlarged detail taken from the images of Figures 12-13, improvements in image definition are quite evident; moreover the figures show the re-sampled pixel u, v and the points x, y of the reference quadrilateral for the interpolation. Figure 16 points out the results of the comparison between ARPAT *in situ* measurements and satellite data; every ARPAT measurement is displayed together with the respective SST estimate, computed using ordinary and segmented interpolation algorithms; the locations of measurement sites and their distance from the coast are also indicated.

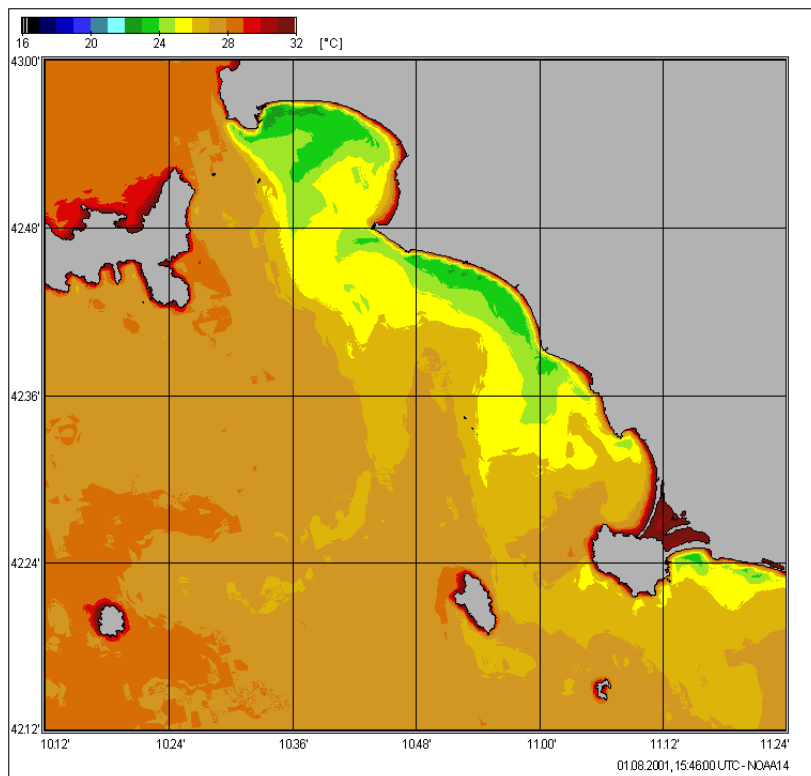


Figure 12: Ordinary interpolation: resampled SST image of the Tuscan Archipelago (Table 3); image of August 1, 2001, UTC 15:46 (NOAA14). The image shows an evident land effect along the coastlines: with ordinary interpolation, the closeness of land to pixels to be interpolated produces a sharp darker border (see Figure 13 for a comparison).

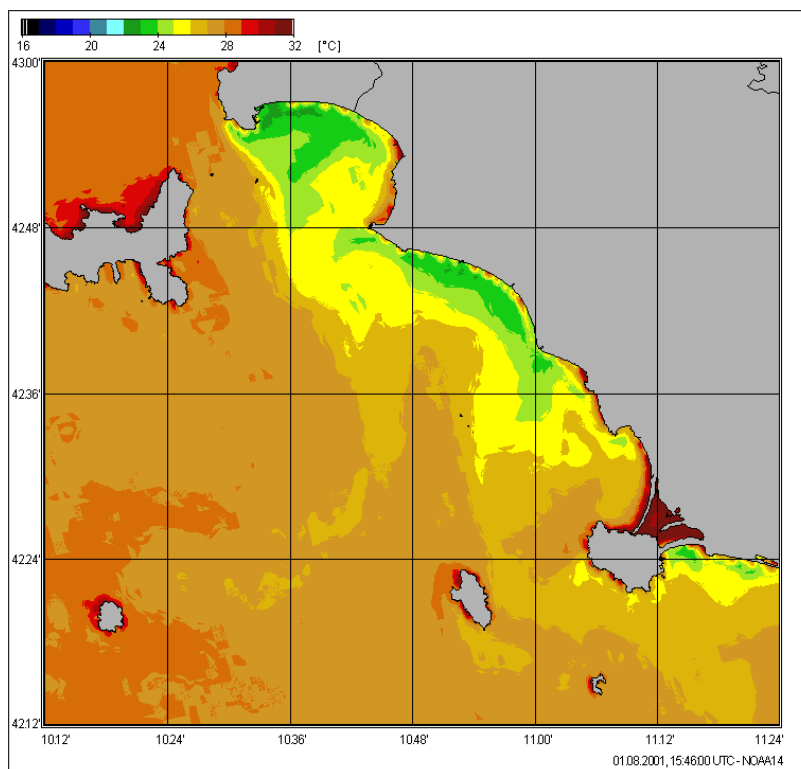


Figure 13: Segmented interpolation: re-sampled SST image of Tuscan Archipelago (Table 3); image of August 1, 2001, UTC 15:46 (NOAA14). Using the proposed algorithm sea pixels along the coastline are re-sampled only using sea unmixed points: the sharp darker border, pointed out in Figure 12, vanishes or is strongly reduced.

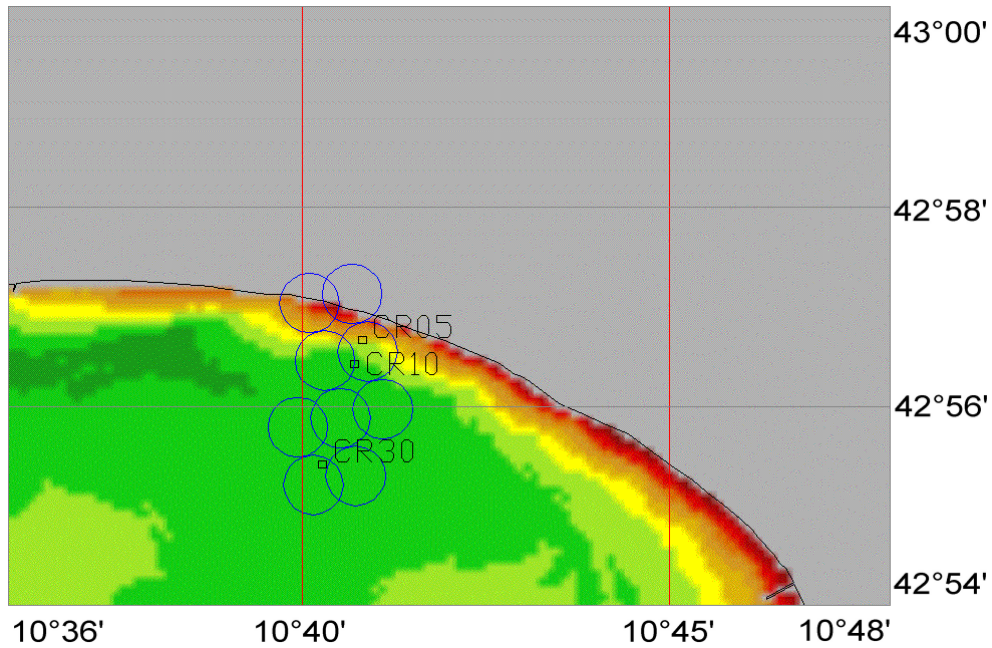


Figure 14: Enlarged detail of the Carbonifera measurement station (Follonica Gulf, see Figure 11) taken from Figure 12: here the circles represent the vertex positions of the acquired NOAA AVHRR14 points used for interpolation; the small squares represent Mercator image pixels whose position is that of the measurement sites CR05, CR10, CR30. AVHRR points, surrounding every pixel, are those used for the interpolation of the pixels.

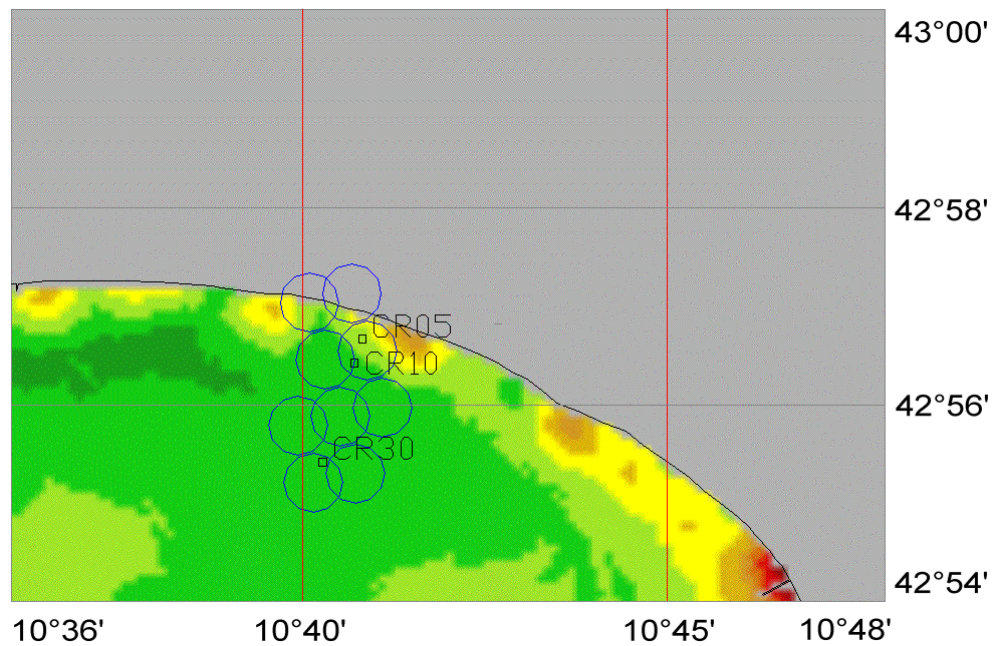


Figure 15: Enlarged detail of the Carbonifera measurement station (Follonica Gulf, see Figure 11) taken from Figure 13: details are the same as in Figure 14.

Unfortunately, it was possible to have simultaneous ARPAT *in situ* data and AVHRR data free from clouds and easy to precisely geo-locate for only 9 measurements (see Table 5). Testings carried out with these *in situ* data are not exhaustive, nevertheless they are quite useful for a first verification of algorithm operation.

In Figure 15 the presence of some warmer zones near the coast is to be noticed. This effect is due to the fact that the segmented algorithm discards and reprocesses those satellite points unsuitable for interpolation. Such a reprocessing is done using close and suitable satellite points. In some

cases these points cannot be considered so close to the point to be reprocessed, thus causing that point to be incorrectly reprocessed. To avoid this problem it is possible to reduce the number of points checked along the eight possible reprocessing directions (e.g., two instead of three, see Figure 4) and also to increase the value of the contamination index threshold (cn_s , see Eq. (3)) so that a satellite point is not discarded even when slightly contaminated. However, these two actions reduce the sharpening effect of the segmented algorithm; this problem is still under discussion and further analysis has to be carried out.

Table 5: ARPAT in situ measurements considered for the comparison of SST data obtained from the AVHRR NOAA14 image from August 1, 2001; UTC 15:46; considered ARPAT measurement stations were Foce Ombrone, Carbonifera and Elba Nord (Figure 11).

Measurement number	Station name	Measurement site	Acquisition date	Acquisition time (UTC)	Distance from coast /m
1	Foce Ombrone	FO30	August 1, 2001	09:01	3000
2	Foce Ombrone	FO10	August 1, 2001	09:25	1000
3	Foce Ombrone	FO05	August 1, 2001	09:29	500
4	Carbonifera	CR30	August 1, 2001	11:22	3000
5	Carbonifera	CR10	August 1, 2001	11:56	1000
6	Carbonifera	CR05	August 1, 2001	12:00	500
7	Elba Nord	EB20	August 1, 2001	13:28	3000
8	Elba Nord	EB10	August 1, 2001	13:55	1000
9	Elba Nord	EB01	August 1, 2001	13:59	100

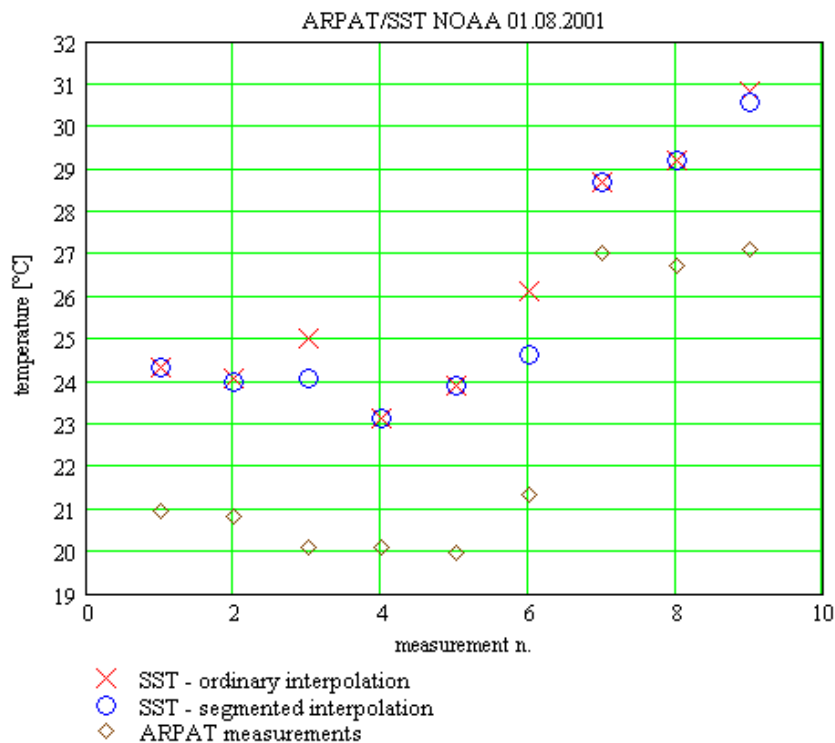


Figure 16: Comparison between in situ measurements performed by ARPAT and SST values obtained, from AVHRR NOAA14 data, with the ordinary and segmented algorithm (all measurements taken August 1, 2001). The considered data are those listed in Table 5.

It can be observed in Figure 16 (considering the distance from the coast of the measurement sites in Table 5) that the segmented algorithm mostly corrects those SST values closest to the coast. For sites whose distance from the coast is more than 1000 m (i.e., about the dimensions of

AVHRR sensor lobe) nearly no correction can be noticed. Generally, the nearer the pixel is to the coast, the more the segmented algorithm corrects.

The main goal of this paper was the improvement of spatial interpolation of SST data near the coast (Figure 8). Nevertheless, during this study a difference between the detected and measured temperature was found. In fact, it can be seen (Figure 16 and also Figure 18) that satellite derived SST values are warmer than those measured *in situ* by about 2-3°C. Although slightly large, such a difference is mostly due to the fact that, for SST evaluation, a standard MCSST (Multi Channel SST) algorithm was used, whose coefficients have a global validity. A mean overestimation of about 2-3°C was found also in the processed AVHRR SST data furnished on line by the Jet Propulsion Laboratory (JPL) of the California Institute of Technology (7).

At present, this problem is still an open problem. The comparative computation for the MCSST algorithm in the Mediterranean Sea area, based on appropriate regional *in situ* measurements, is in progress and is foreseen to be presented in a future publication.

It should also be considered that the *in situ* temperature is taken by ARPAT at a 0.5 m depth, so it is a bulk temperature. This temperature was compared to the SST acquired by the satellite sensor, which is instead a skin temperature. Even if the mean bulk-skin difference is not so high, temperature differences can range from -1.0 to 1.0°C, depending on wind and surface heat flux conditions (8).

Results with boat *in situ* measurements

A further test of the numerical evaluation of SST from AVHRR data with the segmented interpolation algorithm was made also using *in situ* temperature measurements carried out by the sailing boat PIPINA III at 0.5 m of depth. Also in this case, a comparison between SST estimates, obtained with ordinary and segmented algorithm, and the measurements taken at sea, was performed. The selected geographical format for image processing is the *Tuscany* format (see Table 5 and Figure 17).

Figure 17 shows the NOAA16 SST image of May 3, 2003, UTC 11:56 (obtained with segmented interpolation) with the detail of the track carried out from the port of Viareggio to La Spezia with the measurement boat (on x-axis there are minutes from track beginning). The data were acquired May 3, 2003, UTC 8:31-13:52, with an almost continuous sampling of the temperature using an electronic thermometer positioned at 0.5 m under the sea at a distance from the coast varying from 300 to 1000 metres.

The graph of Figure 18 compares PIPINA III sea measurements with SST data derived from AVHRR sensor. For such a comparison the time interval of 80-135 minutes from the campaign track beginning (UTC 9:51-10:46) was considered. During this time interval the measurement boat was sufficiently close to the coast for this purpose (see Figure 17).

Figure 18 shows the comparison between *in situ* measurements carried out by the sailboat PIPINA III along the coastline of Tuscany and the SST values obtained with the ordinary and segmented algorithms. Note that the discrepancy between SST values obtained with ordinary and segmented algorithms can be different from that observed for artificial data (see Table 4 and Figure 8). Such data are created so that the temperature has a linear gradient (Figure 6), which is quite typical. However, if real SST does not behave as in Figure 5, the segmented algorithm can work in a different way from the artificial data case. As for the discrepancy between satellite retrievals and *in situ* measurements, the same considerations of Figure 16 can be made.

CONCLUSIONS AND FUTURE DEVELOPMENTS

An algorithm which improves sea observation from passive satellite remote sensors near the coastline was developed, that can be called *segmented interpolation algorithm*. Algorithm operation was verified using both artificial and real data.

Results obtained with artificial SST data, characterized by a linear temperature gradient (Figure 6), showed, on average, an accuracy improvement of SST retrievals of about 0.3°C.

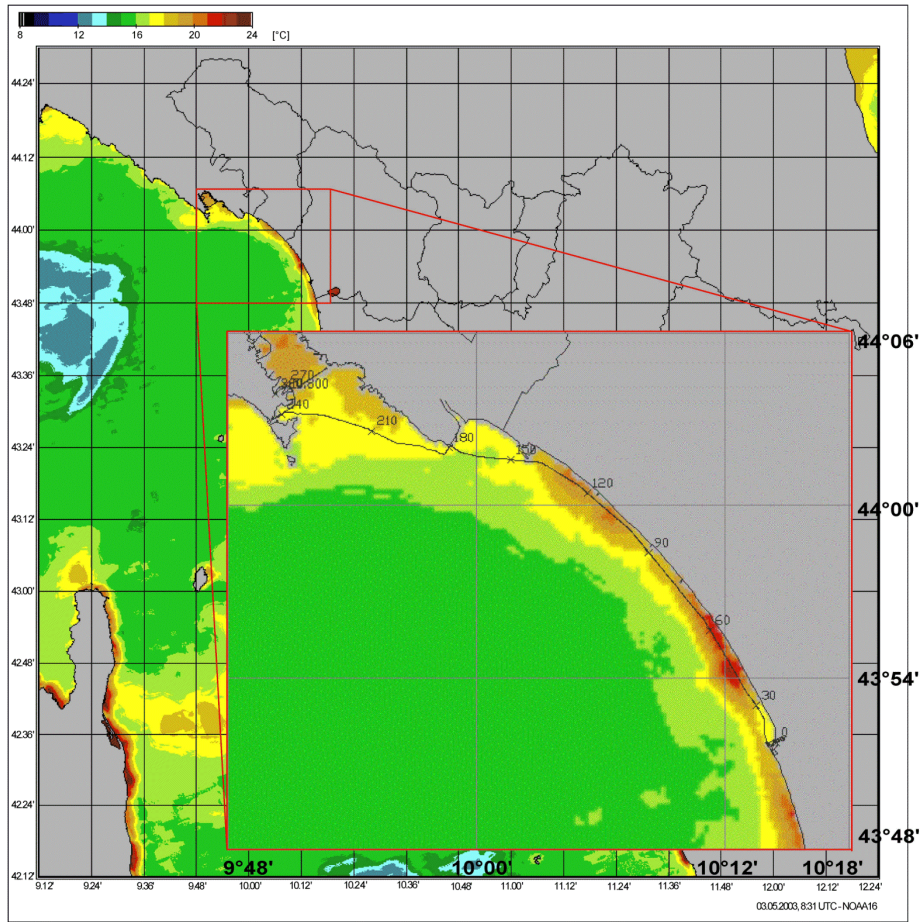


Figure 17: Segmented interpolation: re-sampled SST image of Tuscany (Table 3); image of May 3, 2003, UTC 11:56 (NOAA16). In detail: track of the measurements carried out from the port of Viareggio to La Spezia. Time ticks in the detail represent the minutes from the beginning of the campaign track (May 3, 2003, UTC 8:31).

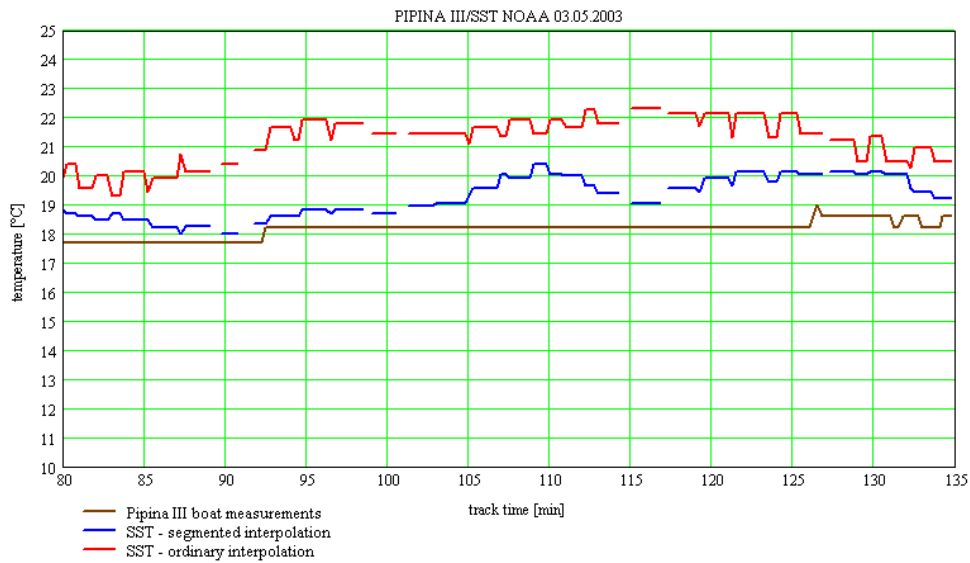


Figure 18: Comparison between in situ measurements carried out by the sailboat PIPINA III along the coastline of Tuscany and the SST values obtained with the ordinary and segmented algorithms. All measurements were taken within the considered time interval (Figure 17), from minute 80 to 135 of the campaign track (May 3, 2003, UTC 9:51-10:46) and at a distance from the coast ranging from 300 to 1000 m; SST data are from May 3, 2003, UTC 11:56 (NOAA16).

Real data were all from AVHRR NOAA14 and NOAA16. An evident enhancement of image definition near the coastline was noticed in the Tuscan Archipelago images from ch.3 counts (Figures 9, 10) and in SST images (Figures 12-15). Using also *in situ* measurements (performed by ARPAT – Regional Agency for the Tuscan Environment – and by the sailboat PIPINA III), a numerical evaluation improvement of SST was demonstrated. Evaluation improvements on image pixels, obtained using the segmented interpolation algorithm, depend on the closeness to the coast of the pixels. In particular, the closer a pixel was to the coast, the more the algorithm corrected its value, if the distance was up to 1000 m (i.e., about the dimensions of AVHRR sensor lobe); whereas, nearly no correction was noticed (Figures 16, 18), when the distance was more than 1000 m.

It is possible to point out some drawbacks and indicate some improvements for the algorithm thus developed.

Points x,y land-sea classification is carried out on the basis of the coastlines, referring to the re-sampling grid u,v . Such an approximation, if a point x,y is placed very close to the coastline, might cause some pixel classification errors. However, if a sea point x,y , which is very close to the coastline (and thus mixed), is badly classified as a land or coast point, it would nevertheless not be considered suitable for interpolation and then reprocessed.

The contamination index for a point x,y acquired by satellite, was computed approximating the satellite sensor lobe (AVHRR in this case) with a square matrix made up of re-sampling grid pixels, so that the matrix side corresponded to the sensor lobe major axis as closely as possible (1.1 km). Considering that the side of the matrix should have an odd number of pixels, it may happen that the approximation will not always be satisfying; to improve the approximation, a model where the sensor lobe ellipticity is taken into account, could be considered.

The segmented interpolation algorithm reprocesses z coordinate of points x,y that are unsuitable for interpolation, using the closest suitable points' z coordinates. In some cases, this method can cause the presence of warmer zones, as noticed and discussed in the obtained results (Figure 15), that can lead to slight errors in the evaluation of the physical parameter of interest. To avoid this problem it is possible to increase the contamination index threshold value (cn_s) and reduce the number of points checked along the reprocessing directions (see results), even if these actions reduce the sharpening effect of the proposed method.

Finally, it is possible to improve SST evaluation from AVHRR data considering some additional environmental parameters that influence the retrievals. For example, water currents, wind speed and also more precise measurements of the water vapour column could be considered (9,10), especially during the summer time.

The *Segmented Interpolation Algorithm* can also be applicable to other satellite sensor data (such as ENVISAT, MODIS or SeaWiFS).

ACKNOWLEDGEMENTS

This work was carried out in cooperation and with the support of the Regional Agency for the Tuscan Environment (ARPAT – Protection of Marine and Coastal Environment Area).

REFERENCES

- 1 Garcia-Consuegra J, G Cisneros & J A Gallud, 1999. Edge pixel classification at subpixel accuracy through resolution enhancement and deconvolution processing, in *Landsat-TM imagery*. In: *IGARSS '99 Proceedings Geoscience and Remote Sensing Symposium*, Volume 1, 1999, 128–130

- 2 Wu H-H P & R A Schowengerdt, 1993. Improved estimation of fraction images using partial image restoration. In: IEEE Transactions on Geoscience and Remote Sensing, Volume 31, Issue: 4, July 1993, 771–778
- 3 Khotanzad A & J-Y Chen, 1989. Unsupervised segmentation of textured images by edge detection in multidimensional feature. In: IEEE Transactions on Pattern Analysis and Machine Intelligence, Volume 11, Issue: 4, April 1989, 414–421
- 4 Murad Agha A K, R Ward & S Zahir, 1999. Image expansion using segmentation-based method. In: IEEE Pacific Rim Conference on Communications, Computers and Signal Processing, 1999, 95–98
- 5 Sakalli M, Y Hong & A M N Fu, 1999. A fuzzy-Bayesian approach to image expansion. In: International Joint Conference on Neural Networks. IJCNN '99, Volume 4, 2685–2689
- 6 Goodrum G, K B Kidwell & W Winston, 2001. NOAA KLM User's Guide. National Oceanic and Atmospheric Administration, Sept 2001
- 7 POET (PO.DAAC Ocean ESIP Tool), 2004. Jet Propulsion Laboratory (JPL), California Institute of Technology (NASA/JPL PO.DAAC) © 1999-2004; <http://poet.jpl.nasa.gov/>
- 8 Schluessel P, W J Emery *et al.*, 1990. On the bulk-skin temperature difference and its Impact on satellite remote sensing of sea surface temperature. Journal of Geophysical Research, 95(C8), 13341-13356
- 9 Emery W J, Y Yu, G A Wick, et al. Correcting infrared satellite estimates of sea surface temperature for atmospheric water vapour attenuation. Journal of Geophysical Research, 99, 5219-5236
- 10 Emery W J & C J Donlon, 1996. Wind speed forcing of the bulk-skin sea surface temperature difference. In: IEEE IGARSS '96 conference, Lincoln, Nebraska, May 1996